Modern Physics Letters A
(2024) 2450137 (16 pages)

DOI: 10.1142/S0217732324501372

Polarization effects of hot nuclear matter on the fusion of heavy ions

R. Gharaei *,†,‡, S. Ramezani Sani* and H. A. Rahnamaye Aliabad*

*Department of Physics, Sciences Faculty, Hakim Sabzevari University, P.O. Box 397, Sabzevar, Iran

†Department of Physics, Faculty of Science, Ferdowsi University of Mashhad, P.O. Box 91775-1436, Mashhad, Iran

‡r.gharaei@hsu.ac.ir

Received 10 May 2024
Revised 22 July 2024
Accepted 2 August 2024
Published 17 September 2024

Within the framework of the modified density-dependent Seyler–Blanchard approach in the T^2 approximation, the polarization effects of hot nuclear matter (PEHNM) are investigated on the fusion process of 16 different colliding systems in the mass range $96 \leq Z_1 Z_2 \leq 850$. In order to calculate the nucleus–nucleus potential, we use the double-folding (DF) model supplemented with the thermal effects of compound nucleus and also a repulsive potential that takes into account the incompressibility of the nuclear matter. The calculations of the fusion cross-sections are performed based on the couplings to the low-lying 2^+ and 3^- vibrational states in both target and projectile. The sensitivity of sub-barrier fusion cross-sections to the polarization effects is evident from this study. The obtained results reveal that the modified form of the DF potential in the presence of the PEHNM appropriately reproduces the energy-dependent behavior of the experimental fusion cross-sections for the studied reactions. The role of the polarization effects on the fusion barriers as well as the inner part of the potential is also discussed.

Keywords: Heavy-ion fusion reactions; Seyler–Blanchard approach; double-folding model; polarization effects.

PACS Nos.: 25.70.Jj, 21.65.Mn, 24.70.+s

1. Introduction

Nuclear matter is an infinite system of nucleons with a definite neutron–proton ratio. To describe the static and thermal properties of nuclear matter, one can use the equation of state at zero (or finite) temperature.[1–8] The equation of state predicted by the Thomas–Fermi model is a simple and useful approach to study the different

‡Corresponding author.

properties of nuclear matter.[9] It has also been used in interpreting the nucleus–nucleus collisions at low incident energies. For example, the authors of Refs. 10–13 simulated the saturation effects of cold nuclear matter in the nucleon–nucleon interactions using a short-ranged repulsive potential in the framework of the Thomas–Fermi model. It is shown that these physical effects play a vital role in achieving a satisfactory description of the heavy-ion fusion cross-sections at energies far below the Coulomb barrier. Seyler–Blanchard potential[14] is another theoretical framework for presenting the nuclear equation of state and thus studying the properties of nuclear matter. In the last few years, a modified density-dependent Seyler–Blanchard potential[15] has been proposed to study the equation of state of hot polarized nuclear matter (HPNM). It is remarkable that Dabrowski and Haensel[16,17] have basically studied the polarized nuclear matter at zero temperature. The various properties of hot polarized nuclear matter at finite temperatures have been studied by Hassan and co-workers.[5] In Refs. 18 and 19, the hot nuclear matter equation of state based on the density-dependent Seyler–Blanchard formalism at finite temperatures[20] has been employed to discuss the temperature dependence of a repulsive core potential in the nucleon–nucleon interactions for four colliding systems including ^{40}Ar+^{40}Ca, ^{28}Si+^{40}Ca, ^{35}Cl+^{48}Ti, and ^{40}Ar+^{74}Ge. Assuming that the compound nucleus (CN) to be a finite piece of hot nuclear matter, this approach provides equation of state for calculating the energy per particle of hot nuclear matter after complete overlap of the two colliding nuclei. To address the experimental fusion excitation functions, the authors considered the couplings to internal structure degrees of freedom of the projectile and target using the coupled-channels (CC)[21] analysis. Based on the thermal predictions obtained for the interaction potential and fusion cross-sections, one can conclude that the thermal effects of compound nucleus play a significant role in improving the agreement between the theoretical and experimental values of the fusion cross-sections for the considered colliding systems. Recently, Ghorbani *et al.*[22] analyzed the effect of inclusion of the repulsive nuclear potential and its temperature dependence on the calculations of the fusion cross-section within the framework of the DF potential accompanied by the Thomas–Fermi model for the reactions ^{18}O+^{63}Cu, ^{18}O+^{194}Pt, ^{16}O+^{208}Pb, and ^{12}C+^{141}Pr. They introduced a temperature-dependent form for this part of nuclear potential. It is shown that the agreement between the calculated and measured values of the fusion cross-sections is increased by including the repulsive nuclear potential.

From the physical point of view, the two possible spin orientations of nucleons can be responsible for the polarization effects of hot nuclear matter. We note that the equation of state predicted by the modified density-dependent Seyler–Blanchard potential at finite temperature contains the volume E_V, symmetry E_X, spin symmetry E_Y, and spin–isospin symmetry E_Z terms,[15] which will be described in the following section. Therefore, it allows us to investigate the effects of neutron excess and also spin-polarization of HPNM on the fusion process of heavy ions. In the previous works,[18,19] we only considered the influence of the volume E_V and

symmetry E_X terms on the fusion reactions. In such situations, the study of the role of spin-polarization effects of HPNM on the various characteristics of the fusion reaction, especially on the energy-dependent behavior of experimental cross-sections, is a completely new topic in the nuclear physics theory. Therefore, we try for the first time to investigate the importance of these effects in the fusion of heavy ions by entering the E_Y- and E_Z-dependent terms in the calculations of the energy per particle of HPNM. We calculate the internuclear potential by applying the M3Y-DF potential which has been modified with a repulsive core term that simulates the effect of nuclear incompressibility. In addition, the theoretical values of the fusion cross-section are calculated within the framework of the CC mechanism, including couplings to the low-lying 2^+ and 3^- states in the target and projectile.

In Sec. 2, we outline the DF model that is employed to calculate ion–ion potential and the repulsive core potential as well as the equation of state of HPNM. Section 3 contains the results and discussion. Section 4 is devoted to some concluding remarks.

2. Theoretical Framework

2.1. *Internuclear potential*

The double-folded nuclear interaction potential between projectile and target can be calculated by[23,24]

$$V_{\rm DF}(\mathbf{R}) = \int d\mathbf{r}_1 \int d\mathbf{r}_2 \rho_1(\mathbf{r}_1)\rho_2(\mathbf{r}_2)\upsilon_{\rm NN}(\mathbf{r}_{12} = \mathbf{R} + \mathbf{r}_2 - \mathbf{r}_1), \tag{1}$$

where R is the distance between the centers of the two colliding nuclei. We notice that the basic inputs in calculating the DF integral are the realistic effective nucleon–nucleon interaction $\upsilon_{\rm NN}$ and the nuclear density distributions $\rho_{1(2)}$ of the projectile and target. The former part can be estimated using the M3Y-Paris effective interactions with a zero-range approximation for the exchange part of the nucleon–nucleon interaction.[25] The direct part of this effective NN interaction can be written as follows:

$$\upsilon_{\rm dir}(\mathbf{r}_{12}) = \upsilon_{00}(\mathbf{r}_{12}) + \frac{N_1 - Z_1}{A_1}\frac{N_2 - Z_2}{A_2}\upsilon_{01}(\mathbf{r}_{12}), \tag{2}$$

which depends on isospin for reactions with $N \neq Z$. To calculate the exchange term in the nuclear potential, which takes into account the effect of antisymmetrization under the exchange of nucleons between the two nuclei, we can use the following relation:

$$\upsilon_{\rm ex}(\mathbf{r}_{12}) = \left(\widehat{J}_{00} + \frac{N_1 - Z_1}{A_1}\frac{N_2 - Z_2}{A_2}\widehat{J}_{01}\right)\delta(\mathbf{r}_{12}). \tag{3}$$

Two-parameter Fermi–Dirac (2PF) distribution function within the framework of the frozen approximation has been commonly used to parameterize the nucleon

densities $\rho_{1(2)}$ as follows:

$$\rho_i^{\mathrm{2PF}}(r) = \frac{\rho_0}{1 + \exp\left(\frac{r - R_{0i}}{a}\right)}, \tag{4}$$

where the average radius $R_{0i} = r_{0i} A_i^{1/3}$. The parameters ρ_0 and a represent the saturation density and surface diffuseness of nuclear matter distribution, respectively. The values of these parameters are taken from a compilation of elastic electron scattering data.[26]

As a result of the literature, several authors pointed out that the original M3Y parametrization for the nucleon–nucleon interactions predicts correctly the ion–ion potential only for peripheral collisions. In fact, it is shown that the microscopic M3Y double-folding potential cannot obtain a satisfactory description of the extreme sub-barrier energies. A fact which confirms the existence of a shallow pocket of the potential in the inner part of the fusion barrier. To cure this deficiency, one needs to supplement the calculations this theoretical model with an effective contact interaction as $\upsilon_{\mathrm{rep}}(\mathbf{r}_{12}) = V_{\mathrm{rep}}\delta(\mathbf{r}_{12})$ that takes into account the saturation effects of cold nuclear matter. According to the recipe proposed in Refs. 10 and 11, the repulsive potential is proportional to the overlapping volume of the reacting nuclei as follows:

$$V_{\mathrm{rep}}(\mathbf{R}) = V_{\mathrm{rep}} \int d\mathbf{r}_1 \int d\mathbf{r}_2 \rho_1(\mathbf{r}_1)\delta(\mathbf{r}_{12})\rho_2(\mathbf{r}_2), \tag{5}$$

where V_{rep} denotes the strength of the repulsive interaction. The densities that appear in the above integral relation are parameterized with Fermi–Dirac distribution functions, Eq. (4). Remarkably, we use the relatively sharp density profiles characterized by the diffuseness parameter a_{rep} to determine these density distributions and thus calculate the repulsive potential from the double-folding integral. In order to access the values of the parameter a_{rep}, we consider the agreement between the theoretical and experimental fusion cross-sections. In fact, this parameter at each incident energy is adjusted for a given value of the strength of the repulsive term V_{rep} so that the best agreement with the experimental cross-sections is achieved. We note that in this work, the influence of the spin-polarization of hot nuclear matter has only been considered on the strength of the repulsive core potential (namely the V_{rep} parameter). This means we assume that the diffuseness parameter a_{rep} is independent from the polarization effects.

2.2. *Equation of state of hot polarized nuclear matter*

Polarized nuclear matter is composed of number $P\uparrow(P\downarrow)$ of spin-up (spin-down) protons and $N\uparrow(N\downarrow)$ spin-up (spin-down) neutrons. Under these conditions, the total number A of particles is given by

$$A = P\uparrow + P\downarrow + N\uparrow + N\downarrow. \tag{6}$$

The corresponding densities are $\rho_{p\uparrow}$, $\rho_{p\downarrow}$, $\rho_{n\uparrow}$, and $\rho_{n\downarrow}$. Thus, the total density $\rho = \rho_p + \rho_n$ can be written as

$$\rho = \rho_{p\uparrow} + \rho_{p\downarrow} + \rho_{n\uparrow} + \rho_{n\downarrow}. \tag{7}$$

The three parameters X (neutron excess parameter), Y (spin-up nucleon excess parameter), and Z (spin-up neutron excess parameter) are defined for polarized nuclear matter as follows:

$$X = \frac{N\uparrow + N\downarrow - P\uparrow - P\downarrow}{A}, \tag{8}$$

$$Y = \frac{N\uparrow - N\downarrow + P\uparrow - P\downarrow}{A}, \tag{9}$$

$$Z = \frac{N\uparrow - N\downarrow - P\uparrow + P\downarrow}{A}, \tag{10}$$

where the Y and Z parameters are a measure of the asymmetric and polarization specifications of the HPNM. Within the framework of Seyler–Blanchard approach, the energy per particle of HPNM at finite temperature T can be written in a simple form[27]

$$E(\rho, T) = E_0(\rho, T = 0) + E_T(\rho, T), \tag{11}$$

where $E_0(\rho, T = 0)$ is the total energy per nucleon at $T = 0$.[9] It can be defined as

$$E = E_V + X^2 E_X + Y^2 E_Y + Z^2 E_Z, \tag{12}$$

E_V, E_X, E_Y, and E_Z are, respectively, the volume, symmetry, spin symmetry, and spin–isospin symmetry energies. These energies are given by

$$E_V = \frac{3\hbar^2 C^{2/3}}{10m}\rho^{2/3} + \left(-\frac{a^3 C}{3\pi}\rho + \alpha\frac{a^3 2^n C}{3\pi}\rho^{n+1} + \frac{2a^3 C^{5/3}}{5\pi b^2}\rho^{5/3} - \beta\frac{2a^3 C^{2/3}}{5\pi}\rho^{2/3}\right)C_1 \tag{13}$$

and

$$E_i = \frac{\hbar^2 C^{2/3}}{6m}\rho^{2/3} - \frac{a^3 C}{3\pi}\rho C_{i1} + \alpha\frac{a^3 2^n C}{3\pi}\rho^{n+1}C_{i1} + \frac{4a^3 C^{5/3}}{9\pi b^2}\rho^{5/3}C_{i2} - \beta\frac{2a^3 C^{2/3}}{9\pi}\rho^{2/3}C_{i3}, \tag{14}$$

where $i = X, Y$, and Z and $C = 3\pi^2/2$. Here, m is the nucleon mass. The values of $a, b, \alpha, \beta, n, C_1, C_{i1}, C_{i2}, C_{i3}$ based on the modified Seyler–Blanchard potential are tabulated in Table 1.

In order to calculate the temperature-dependent part of the energy per nucleon $E_T(\rho, T)$ in the T^2 approximation in Eq. (11), one can use the following definition[20]:

$$E_T(\rho, T) = -\frac{T^2}{6}\left(\frac{2m^*}{\hbar^2}\right)\left(\frac{3\pi^2}{2}\right)^{1/3}\rho^{-2/3}, \tag{15}$$

Table 1. Parameters of the modified Seyler–Blanchard potential, Eqs. (13) and (14), which have been used in calculating the volume, symmetry, spin symmetry, and spin-isospin symmetry energies.[20]

$a = 0.565\,\text{fm}$	$b = 9.678\,\text{fm}^{-1}$	$\alpha = 0.956$
$\beta = 0$	$n = 1/3$	$C_1 = 2393.1$
$C_{X1} = -1357.1$	$C_{X2} = -839.1$	$C_{X3} = -3232.2$
$C_{Y1} = -1211.9$	$C_{Y2} = -621.3$	$C_{Y3} = -3014.4$
$C_{Z1} = -1515.7$	$C_{Z2} = -1077$	$C_{Z3} = -3470.1$

where m^* is the nucleon effective mass and is given by

$$m^* = m\left[1 + \frac{m}{\hbar^2}\left(\frac{4a^3ck_f^3}{3\pi b^2}\right)\right]^{-1}, \tag{16}$$

where k_f is the Fermi momentum. In order to calculate the temperature values T of the CN related to its excitation energy E^*_{CN}, one can use the following relation[28,29]:

$$E^*_{\text{CN}} = Q_{\text{in}} + E_{\text{c.m.}} = \frac{1}{9}AT^2 - T, \tag{17}$$

where A and Q_{in} are the mass number and entrance (incoming) channel Q-value.

2.3. *Estimation of the repulsive core parameters*

The well-known result of sudden approximation is that when two nuclei overlap each other, the nuclear matter density increases in the overlapping region up to $\rho = 2\rho_0$. As a direct consequence of the definition of equation of state, the increase of the density in the overlapping region leads to an increase ΔU in the energy of the nucleons of compound (fused) system. By considering the thermal dependence of the CN, the increasing energy of the system can be calculated by[18,19]

$$\Delta U(T) \approx 2A_P[E(\rho \simeq 2\rho_o, T) - E(\rho \simeq \rho_o, T = 0)], \tag{18}$$

where A_P is the mass number of the projectile nucleus. The equation of state introduced by Myers and Swiatecki can be used to estimate the total energy per particle $E(\rho, T = 0)$ of cold nuclear matter.[9] Within the framework of the Thoms–Fermi model, the nuclear equation of state is defined in the form of a three-term polynomial in the cube root of the nuclear density $\rho = \rho_n + \rho_p$ as follows:

$$\varepsilon(\rho, \delta) = \varepsilon_F\left[A(\delta)\left(\frac{\rho}{\rho_0}\right)^{2/3} + B(\delta)\left(\frac{\rho}{\rho_0}\right) + C(\delta)\left(\frac{\rho}{\rho_0}\right)^{5/3}\right], \tag{19}$$

with coefficients that are functions of the relative neutron excess $\delta = (\rho_n - \rho_p)/\rho$. In this relation, $\rho_0 = 0.161\,\text{fm}^{-3}$ is the saturation density and ε_F is the Fermi energy of nuclear matter. The detailed expressions for the δ dependence entering the above equation are presented in Ref. 9. In addition, the energy $E(\rho, T)$ is obtained from

Eq. (11). From the theoretical point of view, one can use the following condition in order to estimate the strength $V_{\rm rep}$ of the repulsive interaction in the complete overlapping region of density distributions[10,11]

$$V_N(R=0) = [V_{\rm atr}(R) + V_{\rm rep}(R)]_{R=0} = \Delta U(T), \tag{20}$$

where $V_{\rm atr}(R)$ and $V_{\rm rep}(R)$ can be calculated from Eqs. (1) and (5), respectively. In order to estimate the values of the energy $\Delta U(T)$, we must use Eq. (18).

3. Results and Discussion

In the previous studies,[18,19] we analyzed only the influence of the volume energy and neutron excess parameter [X-dependent term in Eq. (12)] on the heavy-ion fusion reactions. Here, our main concern is to investigate the role of the PEHNM on the various characteristics of fusion by considering the influence of spin-up nucleon excess and spin-up neutron excess parameters (Y- and Z-dependent terms). In order to obtain information on this topic, we analyze fusion processes in 16 collisions, including ^{16}O+^{26}Mg$\rightarrow^{42}$Ca, ^{16}O+^{63}Cu$\rightarrow^{79}$Rb, ^{18}O+^{24}Mg$\rightarrow^{42}$Ca, ^{18}O+^{63}Cu$\rightarrow^{81}$Rb, ^{18}O+^{92}Mo$\rightarrow^{110}$Sn, ^{27}Al+^{45}Sc$\rightarrow^{72}$Sc, ^{27}Al+^{72}Ge$\rightarrow^{99}$Rh, ^{28}Si+^{28}Si$\rightarrow^{56}$Ni, ^{28}Si+^{30}Si$\rightarrow^{58}$Ni, ^{28}Si+^{58}Ni$\rightarrow^{86}$Mo, ^{32}S+^{24}Mg$\rightarrow^{56}$Ni, ^{32}S+^{40}Ca$\rightarrow^{72}$Kr, ^{35}Cl+^{24}Mg$\rightarrow^{59}$Cu, ^{35}Cl+^{48}Ti$\rightarrow^{83}$Y, ^{35}Cl+^{124}Sn$\rightarrow^{159}$Ho, and ^{40}Ca+^{40}Ca$\rightarrow^{80}$Zr with $96 \leq Z_1 Z_2 \leq 850$. The compound nuclei formed in the different fusion reactions are highly excited nucleon systems. They can thus be considered as a piece of hot polarized nuclear matter. In this situation, one can determine the number of spin-up or spin-down protons or neutrons for different compound nuclei. Accordingly, there is a considerable interest in performing research on the X, Y, and Z parameters. In this work, the values of these parameters are calculated based on the nuclear shell model for all the compound nuclei of interest. The main feature of this model is similar to the atomic shell model except that the conventional Woods–Saxon (WS) parametrization accompanied by the spin–orbit potential $V_{\rm so}(r)l.s$ was used for the shell-model potential. In addition, we note that the nuclear shell model utilizes the Pauli exclusion principle to model the structure of atomic nuclei in terms of the energy level. Our results show that the calculated values are ranged as $0.0 \leq X \leq 0.20$, $0 \leq Y \leq 0.09$, and $0.41 \leq Z \leq 0.53$. The obtained results with more details are shown in Fig. 1 as a function of $A_1^{1/3} + A_2^{1/3}$. One can see that the X and Z parameters increase and decrease with increasing $A_1^{1/3} + A_2^{1/3}$ quantity, respectively. While Y does not change significantly. So it seems that among the two parameters Y and Z which are responsible for the polarization effects, the contribution of spin-up neutron excess parameter in heavy-ion fusion reactions is greater than the spin-up nucleon excess parameter. Although this result is reasonable on physical grounds, the compound nuclei produced in the present heavy-ion fusion reactions are neutron-rich nuclei.

Figure 2 shows a comparison of the various versions of total interaction potentials calculated within the framework of the DF model for the fusion of the ^{16}O+^{26}Mg, ^{27}Al+^{45}Sc, ^{28}Si+^{58}Ni, ^{32}S+^{24}Mg, ^{18}O+^{92}Mo, ^{18}O+^{24}Mg, ^{40}Ca+^{40}Ca, and ^{16}O+^{63}Cu

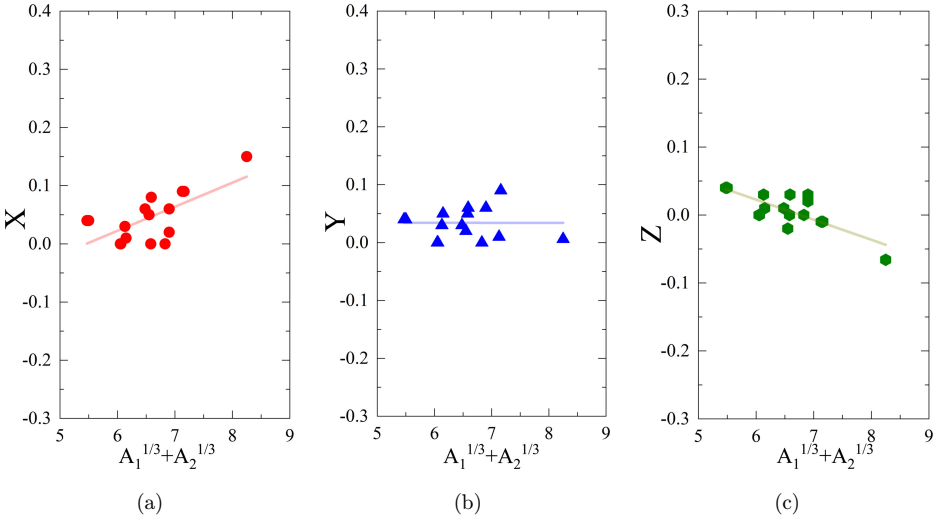

Fig. 1. (Color online) Variation trend of the calculated values of parameters (a) X, (b) Y, and (c) Z vs. $A_1^{1/3}+A_2^{1/3}$ quantity for all the fusion systems considered in this paper.

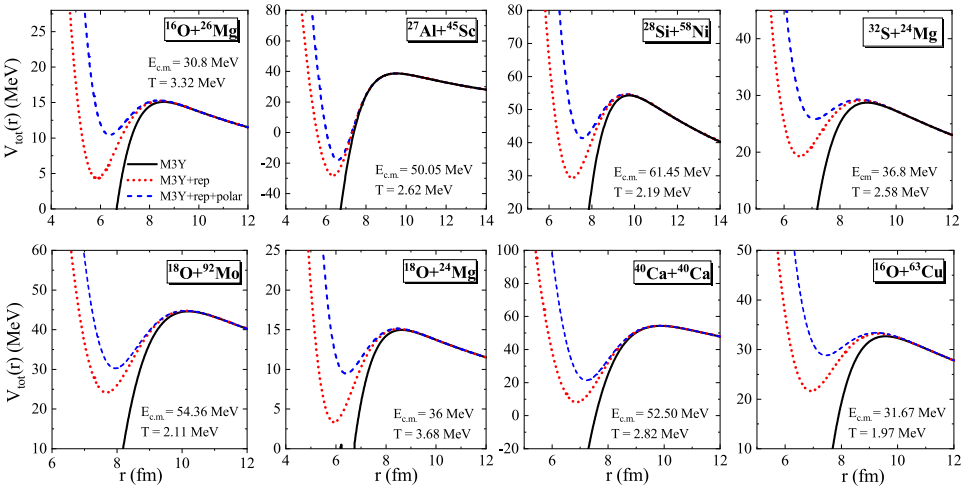

Fig. 2. (Color online) The M3Y+repulsion potential (with and without the polarization effects) is compared to the pure M3Y potential for eight different colliding systems as examples. The values of temperature T (equivalently the incident energy $E_{c.m.}$) have also been presented in each panel.

systems as examples. Because of an abrupt decrease at small ion–ion distances, one can conclude that the Coulomb plus the nuclear M3Y-DF (CDM3Y6) potentials (solid lines) generate an unphysical profile — a fact that has already been mentioned in the literature.[10,11,30,31] It is also clear from the figure that by considering the repulsive interaction which simulates the effect of saturation properties of the hot

nuclear matter, a rather shallow pocket in the entrance channel potential can be produced. We mark the results of the modified form of the DF potential as "M3Y+ repulsion" potential (short-dotted lines). It must be noted that the thermal modifications of the DF model in this step include only the influence of the volume energy and X-dependent terms in Eq. (11). In addition, the calculations of M3Y+repulsion potentials for the above-mentioned reactions are performed at incident energies $E_{\text{c.m.}} = 30.80$ MeV (equivalently $T = 3.32$ MeV), $E_{\text{c.m.}} = 50.05$ MeV (equivalently $T = 2.62$ MeV), $E_{\text{c.m.}} = 61.45$ MeV (equivalently $T = 2.19$ MeV), $E_{\text{c.m.}} = 36.80$ MeV (equivalently $T = 2.58$ MeV), $E_{\text{c.m.}} = 54.36$ MeV (equivalently $T = 2.11$ MeV), $E_{\text{c.m.}} = 36.00$ MeV (equivalently $T = 3.68$ MeV), $E_{\text{c.m.}} = 52.50$ MeV (equivalently $T = 2.82$ MeV), and $E_{\text{c.m.}} = 31.67$ MeV (equivalently $T = 1.97$ MeV), respectively. The obtained results for M3Y+repulsion model reveal that the density distributions used in calculating the repulsive part of the potential have a sharper profile with smaller diffusivity ($a_{\text{rep}} < 0.47$ fm) than the original M3Y parametrization. In Fig. 2, the short-dashed curves are based on the M3Y+repulsion potentials with PEHNM. Herein, we consider the Y- and Z-dependent terms for calculating the total energy per nucleon via Eq. (11). The influence of polarization effects of hot nuclear matter on the inner part of the Coulomb barrier and its thickness is evident. One can find that these effects reduce the depth of the pocket in the entrance channel potential for all the cases of interest. While the fusion barriers are not very sensitive to these physical effects.

Another important quantity in both theoretical and experimental studies of the heavy-ion fusion reactions is fusion cross-section (σ_{fus}). In this study, the values of this quantity have been determined within the framework of the CC method by imposing ingoing-wave boundary conditions at the position of the minimum of pocket in the entrance potential. We include couplings to one-phonon excitations of the low-lying 2^+ and 3^- states in both projectile and target using the computer code CCFULL.[21] In this code, the WS parametrization is adopted for the nuclear interaction potential. By fitting a WS form to the original and modified forms of the M3Y-DF potential at the fusion barrier radii, the equivalent WS potential parameters have been extracted at each bombarding energy. The nuclear structure inputs of these collective states, including excitation energy and corresponding deformation, are reported in Table 2 for reacting nuclei. The influence of the PEHNM on the fusion of different colliding systems is illustrated in Fig. 3 in terms of the ratio of the experimental fusion cross-sections to the results of CC calculations. It is clearly seen that the DF ion–ion potential based on the effective M3Y interaction cannot describe the energy-dependent behavior of the fusion cross-sections in particular at low energies. This figure shows that the obtained results by the M3Y interaction have been improved by supplementing it with a repulsive term for hot nuclear matter. However, it is seen for the selected reactions that the best fit to the data occurs when we use the M3Y+repulsion model with CC+PEHNM calculations. In fact, the ratio of $\sigma_{\text{fus}}^{\text{exp}}/\sigma_{\text{fus}}^{\text{cal}}$ tends to one at the lowest energies by considering the polarization effects on the fusion. Based on the uncertainties that have been reported for experimental

Table 2. The low-lying excited states (λ^{π}) with excitation energies (E^{*}) and corresponding deformation parameters (β_{λ}) used in the CC calculations for all the nuclei we have considered. The data are taken from Refs. 32 and 33.

Nucleus	λ^{π}	E^{*}	β_{λ}
^{16}O	2^{+}	6.917	0.349
	3^{-}	6.130	0.729
^{18}O	2^{+}	1.982	0.348
	3^{-}	5.098	0.595
^{24}Mg	2^{+}	1.368	0.609
	3^{-}	7.616	0.326
^{26}Mg	2^{+}	1.808	0.489
	3^{-}	6.876	0.213
^{27}Al	2^{+}	1.793	0.447
	3^{-}	6.877	0.307
^{28}Si	2^{+}	1.779	0.407
	3^{-}	6.879	0.401
^{30}Si	2^{+}	2.235	0.310
	3^{-}	5.488	0.277
^{32}S	2^{+}	2.230	0.310
	3^{-}	5.006	0.534
^{35}Cl	2^{+}	2.049	0.251
	3^{-}	4.401	0.396
^{40}Ca	2^{+}	3.904	0.106
	3^{-}	3.737	0.411
^{45}Sc	2^{+}	1.023	0.574
	3^{-}	3.183	0.191
^{48}Ti	2^{+}	0.983	0.257
	3^{-}	3.359	0.197
^{58}Ni	2^{+}	1.454	0.176
	3^{-}	4.475	0.198
^{63}Cu	2^{+}	1.082	0.215
	3^{-}	3.377	0.215
^{72}Ge	2^{+}	0.834	0.240
	3^{-}	2.515	0.264
^{92}Mo	2^{+}	1.509	0.106
	3^{-}	2.850	0.166
^{124}Sn	2^{+}	1.131	0.094
	3^{-}	2.603	0.106

fusion cross-sections at different incident energies, one can obtain the upper and lower limit of the errors of the ratio of the experimental to theoretical fusion cross-sections as $(\frac{\sigma_{\rm fus}^{\rm exp}+\delta\sigma_{\rm fus}}{\sigma_{\rm fus}^{\rm cal}}-\frac{\sigma_{\rm fus}^{\rm exp}}{\sigma_{\rm fus}^{\rm cal}})$ and $(\frac{\sigma_{\rm fus}^{\rm exp}-\delta\sigma_{\rm fus}}{\sigma_{\rm fus}^{\rm cal}}-\frac{\sigma_{\rm fus}^{\rm exp}}{\sigma_{\rm fus}^{\rm cal}})$, respectively. The unusual large errors for some fusion systems as shown in the figure can be due to the large uncertainties in the experimental fusion cross-sections.

In order to further understand the role of the spin-polarization effects at low energies, the temperature-dependent behavior of the fusion barrier positions R_B (left panels) and heights V_B (right panels) is displayed in Fig. 4 using the M3Y+repulsion

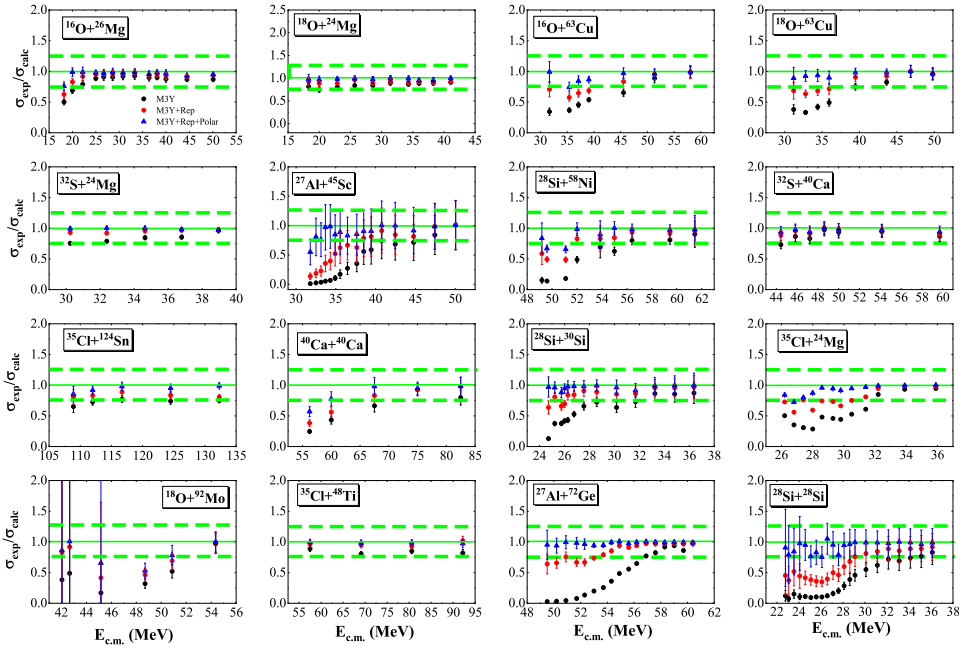

Fig. 3. (Color online) Ratio of experimental to calculated fusion cross-sections using the M3Y-DF, and M3Y+repulsion model with and without the polarization effects for different fusion reactions we investigated in this work.

potential with and without the PEHNM for seven arbitrary fusion systems. The examples shown in this figure are ^{32}S+^{40}Ca, ^{40}Ca+^{40}Ca, ^{35}Cl+^{48}Ti, ^{27}Al+^{45}Sc, ^{28}Si+^{58}Ni, ^{32}S+^{24}Mg, and ^{16}O+^{26}Mg. As mentioned earlier, the sensitivity of the fusion barrier to the polarization effects is low. However, it can be seen from the figure that the imposing of these physical effects increases the height of the Coulomb barrier and thus leads to suppression in the fusion probability. Physical justification for this phenomenon is discussed in the next figure. We also conclude from an inspection of Fig. 4 that the values of R_B and V_B calculated by both theoretical models gradually enhance and reduce by increasing the values of T, respectively. In addition, the difference between the results obtained from the M3Y+repulsion potential with and without the PEHNM increase by decreasing the temperature T (equivalently the incident energy $E_{\rm c.m.}$). This means that the polarization effects play an important role at low incident energies. The increase in the calculated values of the fusion barrier heights can be described satisfactorily by using the temperature-dependent behavior of the strength $V_{\rm rep}$ of the repulsive interaction. Figure 5 (left panels) shows such dependence using the M3Y+repulsion potential with and without the PEHNM for the fusion systems ^{32}S+^{24}Mg and ^{27}Al+^{45}Sc, for example. We can see that the imposing of the polarization effects in the calculations of the total energy per particle of the polarized nuclear matter increases the strength of the repulsive interaction by about 20%. For these two reactions, the diffuseness parameter $a_{\rm rep}$ ranges from

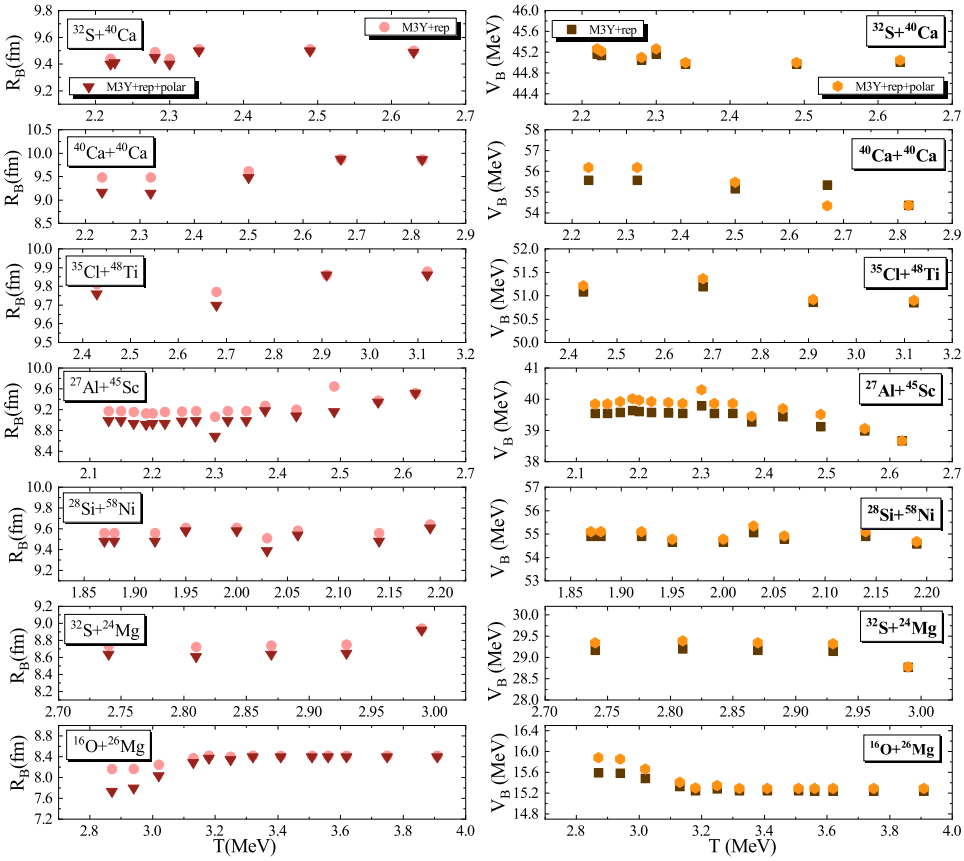

Fig. 4. (Color online) Variations of the calculated values of R_B (left panels) and V_B (right panels) vs. temperature T for the fusion reactions ^{32}S+^{40}Ca, ^{40}Ca+^{40}Ca, ^{35}Cl+^{48}Ti, ^{27}Al+^{45}Sc, ^{28}Si+^{58}Ni, ^{32}S+^{24}Mg, and ^{16}O+^{26}Mg using M3Y+repulsion potential with and without the PEHNM.

0.310 fm to 0.392 fm and from 0.30 fm to 0.402 fm, respectively. In order to further understand the remarkable difference of the repulsive parameter $V_{\rm rep}$ with and without spin-polarization effects, one can mention the observations of Fig. 2. The figure suggests that these effects significantly affect the shape of nuclear potential in the regions inside the barrier. On the other hand, the previous works[31,34] reveal that a close link exists between changing the values of the this parameter and the depth of the pocket. Therefore, it is reasonable that the polarization effects have a significant role in the strength of the repulsive interaction. Another point to note is that the shape of nuclear potential in the regions near the Coulomb barrier radius is also somewhat sensitive toward the change in the repulsive parameter $V_{\rm rep}$.[31,34] In fact, it can be concluded that increasing the values of the repulsive parameter $V_{\rm rep}$ increases the height of the Coulomb barrier in the fusion process. Here and in the following, we are interested in analyzing the temperature dependence of ΔU calculated using Eq. (18) with and without the PEHNM. This is illustrated in Fig. 5

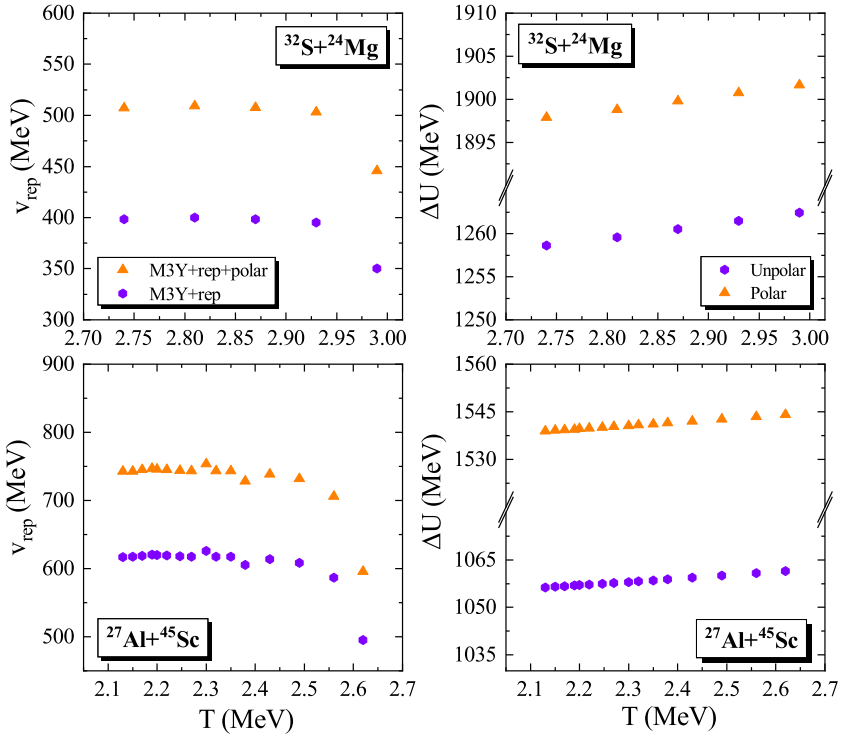

Fig. 5. (Color online) The temperature dependence of the calculated values of the strength $V_{\rm rep}$ of the repulsive interaction (left panels) and the variation of energy ΔU (right panels) using M3Y+repulsion potential with and without the PEHNM for ^{32}S+^{24}Mg and ^{27}Al+^{45}Sc colliding systems.

(right panels) for the above-mentioned systems. It can be seen from this figure that the calculated values of ΔU increase linearly with the increase of the CN temperatures T (equivalently the incident energy $E_{\rm c.m.}$). The results of this figure also confirm that the polarization property of the fused system does not affect the observed behaviors and only increases the calculated values of ΔU by about 30%.

In view of the correlation between the Coulomb barrier height V_B and the repulsive strength parameter $V_{\rm rep}$, it seems that the study of the dependence of these parameters on the center-of-mass energy $E_{\rm c.m.}$ can be useful. Figure 6 shows the calculated values of the parameters V_B (middle panels) and $V_{\rm rep}$ (right panels) using the M3Y+repulsion potential in the presence of the polarization effects as a function of the energy $E_{\rm c.m.}$ for the ^{35}Cl+^{124}Sn, ^{27}Al+^{72}Ge, ^{35}Cl+^{48}Ti, ^{28}Si+^{58}Ni, and ^{18}O+^{92}Mo colliding systems, for example. The energy dependence of the minimum of the potential $V_{\rm pocket}$ (left panels) is also displayed, for comparison. The figure suggests that the three parameters V_B, $V_{\rm rep}$, and $V_{\rm pocket}$ follow a similar trend with the variation of the energy values.

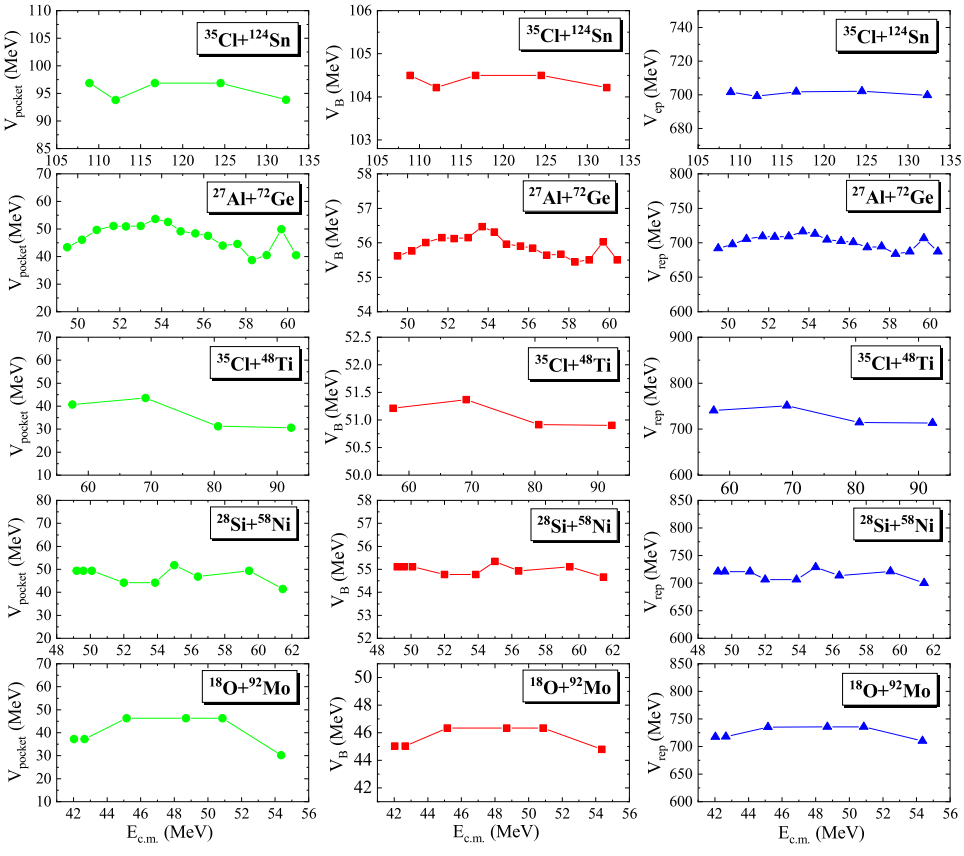

Fig. 6. (Color online) Energy dependence of the three parameters $V_{\rm pocket}$, V_B, and $V_{\rm rep}$ for the ^{35}Cl+^{124}Sn, ^{27}Al+^{72}Ge, ^{35}Cl+^{48}Ti, ^{28}Si+^{58}Ni, and ^{18}O+^{92}Mo fusion systems using the M3Y+repulsion potential with the PEHNM.

4. Conclusions

To summarize, we investigate the spin-polarization effects of hot nuclear matter on the fusion of heavy ions within the framework of the microscopic DF model using realistic nucleon-nucleon interaction. Sixteen colliding systems are taken into account with $96 \leq Z_1 Z_2 \leq 850$ for the charge product of their reacting nuclei. The calculations of the fusion cross-sections are performed using the CC method in which couplings of inelastic channels to fusion have been considered. The main conclusions of this paper can be summarized as follows:

- Using the Seyler–Blanchard approach, the dependence of three parameters X, Y, and Z on the $A_1^{1/3}+A_2^{1/3}$ has systematically been investigated. Our obtained results reveal that the neutron excess and spin-up neutron excess parameters increase and decrease, respectively, with increasing values of $A_1^{1/3}+A_2^{1/3}$, while the parameter Y is not highly sensitive to the change in the mass of the reacting

partners. This implies that the spin-up neutron excess parameter Z plays a decisive role in analyzing the polarization effects in the fusion systems containing neutron-rich nuclei with reference to other parameters.

- Including the PEHNM would lead to an increase of the fusion barrier height and a decrease of the fusion probability for the cases we investigated in this study. From this analysis, we conclude that the depth of the potential in the inner region of the Coulomb barrier decreases by imposing the mentioned effects. The calculated heavy-ion fusion cross-sections for the selected mass range show an acceptable fit to the corresponding experimental data especially at low energies when the Y- and Z-dependent terms are considered to apply the polarization effects in calculating the total energy per nucleon of HPNM.
- This study makes a detailed analysis of the thermal dependence of the various parameters belonging to the M3Y+repulsion potential by considering the polarization effects of hot nuclear matter. The results indicate an apparent correlation between the minimum of the potential pocket V_{pocket}, the barrier height V_B, and the strength of the repulsive-core potential V_{rep}.

ORCID

R. Gharaei https://orcid.org/0000-0003-2256-0028

References

1. K. M. Khanna and P. K. Barhai, *Phys. Rev. C* **11**, 264 (1975).
2. J. Dabrowski, *Nukleonika* **21**, 143 (1977).
3. H. M. M. Mansour and Kh. A. Ramadan, *Phys. Rev. C* **57**, 1744 (1998).
4. H. Jagamma, A. Z. Mekjain and L. Zamick, *Phys. Rev. C* **27**, 2782 (1983).
5. M. Y. M. Hassan, S. S. Montasser and S. Ramadan, *J. Phys. G* **6**, 1229 (1980).
6. W. M. Seif, A. S. Hashem and Y. Ramsis, *Phys. Rev. C* **106**, 015801 (2022).
7. V. Parmar, M. K. Sharma and S. K. Patra, *Phys. Rev. C* **105**, 024316 (2022).
8. W. M. Seif, A. S. Hashem and R. N. Hassanien, *Nucl. Phys. A* **1008**, 122142 (2021).
9. W. D. Myers and W. J. Swiatecki, *Phys. Rev. C* **57**, 3020 (1998).
10. Ş. Mişicu and H. Esbensen, *Phys. Rev. C* **75**, 034606 (2007).
11. Ş. Mişicu and H. Esbensen, *Phys. Rev. Lett.* **96**, 112701 (2006).
12. C. L. Jiang, B. B. Back, K. E. Rehm, K. Hagino, G. Montagnoli and A. M. Stefanini, *Eur. Phys. J. A* **57**, 235 (2021).
13. G. Colucci, G. Montagnoli, A. M. Stefanini, H. Esbensen, D. Bourgin, P. Colovic, L. Corradi, M. Faggian, E. Fioretto, F. Galtarossa, A. Goasduff, J. Grebosz, F. Haas, M. Mazzocco, F. Scarlassara, C. Stefanini, E. Strano, S. Szilner, M. Urbani and G. L. Zhang, *Phys. Rev. C* **97**, 044613 (2018).
14. R. G. Seyler and C. H. Blanchard, *Phys. Rev.* **131**, 355 (1963).
15. D. Bandyopadhyay, C. Samanta, S. K. Samaddar and J. N. De, *Nucl. Phys. A* **511**, 1 (1990).
16. J. Dabrowski and P. Haensel, *Phys. Rev. C* **7**, 916 (1973).
17. J. Dabrowski, *Acta Phys. Pol. B* **7**, 657 (1976).
18. O. N. Ghodsi and R. Gharaei, *Phys. Rev. C* **84**, 024612 (2011).

19. O. N. Ghodsi and R. Gharaei, *Phys. Rev. C* **85**, 064620 (2012).
20. H. M. M. Mansour and Kh. A. Ramadan, *Phys. Rev. C* **57**, 1744 (1998).
21. K. Hagino, N. Rowley and A. T. Kruppa, *Comput. Phys. Commun.* **123**, 143 (1999).
22. F. Ghorbani, S. A. Alavi, V. Dehghani, A. Soylu and F. Koyuncu, *Phys. Rev. C* **102**, 014610 (2020).
23. G. R. Satchler and W. G. Love, *Phys. Rep.* **55**, 183 (1979).
24. D. T. Khoa and G. R. Satchler, *Nucl. Phys. A* **668**, 3 (2000).
25. G. Bertsch, J. Borysowicz, H. McManus and W. G. Love, *Nucl. Phys. A* **284**, 399 (1977).
26. H. de Vries, C. W. de Jager and C. de Vries, *At. Data Nucl. Data Tables* **36**, 495 (1987).
27. H. M. M. Mansour, M. Hammad and M. Y. M. Hassan, *Phys. Rev. C* **56**, 1418 (1997).
28. R. K. Puri and R. K. Gupta, *J. Phys. G* **18**, 903 (1992).
29. R. K. Gupta, S. Singh, R. K. Puri, A. Sandulescu, W. Greiner and W. Scheid, *J. Phys. G: Nucl. Part. Phys.* **18**, 1533 (1992).
30. R. Gharaei, *J. Phys. G: Nucl. Part. Phys.* **44**, 045108 (2017).
31. R. Gharaei and M. R. Yazdi, *Nucl. Phys. A* **1019**, 122381 (2022).
32. S. Raman, C. W. Nestor, Jr. and P. Tikkanen, *At. Data Nucl. Data Tables* **78**, 1 (2001).
33. R. H. Spear, *At. Data Nucl. Data Tables* **42**, 55 (1989).
34. O. N. Ghodsi and V. Zanganeh, *Nucl. Phys. A* **846**, 40 (2010).